The AAPS Journal, Vol. 14, No. 1, March 2012 (© 2011)
DOI: 10.1208/s12248-011-9310-9

Research Article

Comparison of Intestinal Absorption and Disposition of Structurally Similar Bioactive Flavones in *Radix Scutellariae*

Chenrui Li,[1] Li Zhang,[1] Limin Zhou,[1] Siu Kwan Wo,[1] Ge Lin,[2] and Zhong Zuo[1,3]

Received 12 August 2011; accepted 11 November 2011; published online 14 December 2011

Abstract. *Radix Scutellariae* is a commonly used herbal medicine. Baicalein, wogonin, and oroxylin A are three major bioactive flavones in *Radix Scutellariae* and share similar chemical structures. The intestinal absorption and disposition of baicalein have been systematically investigated by our group before. In this study, the intestinal absorption and disposition of wogonin and oroxylin A were further explored and compared with the profiles of baicalein to find potential structure–activity relationship. Absorptive models including Caco-2 cell monolayer model and rat *in situ* single-pass intestinal perfusion model as well as *in vitro* enzymatic kinetic study were employed in the current study. The absorption of baicalein, wogonin, and oroxylin A were favorable with wogonin showing the highest permeability based on two absorptive models. However, three flavones underwent a fast and extensive phase II metabolism. The intestinal metabolism of three flavones exhibited species difference between human and rat. Oroxylin A demonstrated the highest intrinsic clearance of glucuronidation among three flavones. The multidrug resistance proteins might be involved in the efflux of their intracellularly formed conjugated metabolites. The pathway of intestinal absorption and disposition of B, W, and OA was similar. However, the extent of permeability and metabolism was different among three flavones which might be due to the number and position of the hydroxyl group.

KEY WORDS: absorption; baicalein; disposition; oroxylin A; wogonin.

INTRODUCTION

Radix Scutellariae (RS) is commonly used as herbal medicine to treat inflammation, cardiovascular diseases, respiratory, and gastrointestinal infections. As a major ingredient herb, it has been extensively employed in traditional formulations as well as modern medications (1). Baicalein (B), wogonin (W), and oroxylin A (OA) (Fig. 1), sharing a similar backbone of flavone, are three major bioactive flavones in RS. Recent extensive researches demonstrated a variety of pharmacological activities of these flavones including anti-inflammation (2–4), anti-cancer (5,6), anti-viral (7–9), neuroprotective (10–12), as well as anxiolytic effects (13,14).

Similar to the rest of flavonoids, low oral bioavailabilities of the above flavones are expected. Both of Caco-2 cell monolayer model and *in situ* rat intestinal perfusion model have been utilized to investigate the mechanism of their intestinal absorption and disposition. Caco-2 cell monolayer is extensively used because of morphological and functional similarities to human small intestinal epithelium (15). Besides, Caco-2 cells express membrane transporters such as P-glycoprotein (P-gp), multidrug resistance proteins (MRPs), breast cancer resistance protein (BCRP), and organic anion transporters (16–19). There are also metabolic enzymes expressed in the system including cytochrome P450, UDP-glucuronosyltransferase, sulfotransferase, glutathione *S*-transferase, *N*-acetyltransferase, and acyltransferase (20–23). *In situ* rat intestinal perfusion model has advantages over the *in vivo* and *in vitro* models due to its easy control of experiment parameters and exclusion of impact of other organs and the maintain of intact intestinal blood supply (24). Based on our previous studies, B demonstrated favorable permeability across the intestinal epithelium membrane with extensive phase II metabolism in the form of glucuronides and sulfates. MRPs were involved in the efflux of these metabolites (25–27). Sharing the similar backbone of flavone, W and OA might undergo the similar absorptive and metabolic pathways as B. Nevertheless, their intestinal absorption and metabolism have not been compared among three flavones before. The current study aims to investigate the intestinal absorption, disposition, as well as the metabolic kinetic profiles of W and OA and compare that with those of B using *in vitro* Caco-2 cell model, *in situ* intestinal perfusion model, and *in vitro* enzymatic incubation. In addition, the membrane transporters involved in the efflux or influx of intracellularly formed conjugated metabolites of the three flavones, namely baicalin (BG), wogonoside (WG), and oroxylin A-7-*O*-glucuronide (OAG), were identified based on the results from their transport studies in Caco-2 cell model in presence of transporter inhibitors and MDCK cell model transfected with various human transporter genes.

[1] School of Pharmacy, Faculty of Medicine, The Chinese University of Hong Kong, Shatin, New Territories, Hong Kong SAR, China.
[2] School of Biomedical Sciences, Faculty of Medicine, The Chinese University of Hong Kong, Shatin, New Territories, Hong Kong SAR, China.
[3] To whom correspondence should be addressed. (e-mail: joanzuo@cuhk.edu.hk)

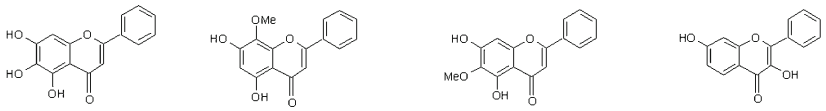

Fig. 1. Chemical structures of baicalein, wogonin, oroxylin A, and 3,7-dihydroxyflavone (internal standard)

MATERIALS AND METHODS

Materials

W and WG with purity over 98% were purchased from AvaChem Scientific LLC (San Antonio, TX, USA). OA (purity over 98%) and OAG (purity over 95%) were supplied by Shanghai u-sea biotech co., Ltd (Shanghai China). Baicalin (BG) was purchased from Aldrich Chem. Co. (Milwaukee, WI, USA). 3, 7-Dihydroxyflavone (IS) as internal standard with purity of 97% was purchased from Indofine Chemical Company (Hillsborough, NJ, USA). Estrone 3-sulfate (ES), estradiol glucuronide (EG), verapamil, and mitoxantrone dihydrochloride (MTX) were purchased from Sigma-Aldrich Chem. Co. (Milwaukee, WI, USA). MK571 was kindly supplied by Merck Frosst Canada & Co. Phenol red, calcium chloride, and sodium dihydrogen phosphate were purchased from BDH chemical Ltd (Poole, England). Potassium chloride, PEG 400, and ascorbic acid were supplied by Wing Hing Chemical Co. (Hong Kong). Potassium dihydrogen phosphate was purchased from Merck (Darmstadt, Germany). Acetonitrile (Labscan Asia, Thailand) and methanol (TEDIA company, Inc., UAS) were HPLC grade and used without further purification. All other reagents were of at least analytical grade. Distilled and deionized water was prepared from Millipore water purification system (Millipore, Milford, MA, USA).

Uridine 5′-diphosphoglucuronic acid (UDPGA), adenosine 3′-phosphate 5′-phosphosulfate (PAPS), and alamethicin were obtained from Sigma-Aldrich Chem. Co. (Milwaukee, WI, USA). Pooled human intestine microsomes (HIM) and pooled male rat intestinal S9 (RIS9, Sprague Dawley) and recombinant human UDP-glucuronosyltransferase (UGT) 1A8 and UGT1A10 were purchased from BD Biosciences (Woburn, MA, USA).

For cell culture, Dulbecco's modified Eagle's medium, fetal bovine serum, 0.25% trypsin–EDTA, penicillin–streptomycin, and non-essential amino acids were purchased from Gibco BRL (Carlsbad, CA, USA) and Life Technologies (Grand Island, NY, USA). Phosphate-buffered saline tablets were purchased from Sigma Chemical Co. (St. Louis, MO, USA).

Cell Lines and Cell Cultures

Caco-2 cells were purchased from American Type Culture Collection. MDCK cell lines used in the experiment were a kind gift from Prof. P. Borst (The Netherlands Cancer Institute). Four types of MDCK cell lines were employed including the wild type of MDCK (MDCK/WT), MDCK cell line transfected with human MDR1 gene (MDCK/MDR1), as well as MDCK cell line transfected with human MRP2 and MRP3 genes (MDCK/MRP2 and MDCK/MRP3). For cell culture, Caco-2 and MDCK cells were cultured in Dulbecco's modified Eagle's medium at 37°C, supplemented with 10% fetal bovine serum, 1% non-essential amino acids, in an atmosphere of 5% CO_2, and 90% relative humidity. Caco-2 cells were subcultured at 70–80% confluence by trypsinization with 0.25% trypsin–EDTA and plated onto six-well plates Transwell® inserts (24 mm I.D., 0.4 mM pore size, 4.71 cm^2, polycarbonate filter, Corning Costar Co., Corning, NY, USA) coated with a collagen layer at a density of 3×10^5 cells/well and cultured for 21 days prior to transport studies. For MDCK cells, the seeding density was 2×10^6 cell/well and cells were cultured for 3 days before transport study. Transepithelial electrical resistance (TEER) was used to monitor the integrity of the Caco-2 and MDCK cell monolayer. Caco-2 monolayers with TEER above 600 Ωcm^2 and MDCK monolayers with TEER above 150 Ωcm^2 were employed in the transport study.

Transport Studies in Caco-2 and MDCK Cell Monolayer Model

Caco-2 cell monolayer grown for 21 days was rinsed twice and equilibrated with transport buffer at 37°C for 15 min before experiment. The transport study of W/OA and WG/OAG was conducted in a bidirectional way and the procedures followed our previous methods (26).

To identify the potential membrane transporters, various transporter inhibitors or substrates at appropriate concentrations were preloaded into both sides for 30 min. Then B to A transport of WG/OAG (2.17 μM) were conducted in the presence of selected inhibitors following the similar procedure as described previously (26).

To further identify potential transporters, the B to A transport study of BG/WG/OAG was carried out in MDCK/WT, MDCK/MDR1, MDCK/MRP2, and MDCK/MRP3 cell lines. Cells grown for 3~4 days were rinsed twice and equilibrated with transport buffer at 37°C for 15 min before experiment. BG/WG/OAG at the concentrations of 2.17 μM in PBS^+ were loaded into the basolateral side followed by B to A transport study as the procedure above. All the samples were stabilized with 0.2 ml mixture of methanol/20% ascorbic acid solution (1:1, *v:v*) and stored at −80°C until analysis.

Investigation of Intestinal Absorptions Using Rat Single-Pass Intestinal Perfusion Model

Male Sprague Dawley rats, weighing 230 to 250 g, were used in current studies. The rat surgery and the preparation of perfusate buffer were similar to our previous methods (25). The perfusion buffer containing 50 μM of W or OA was perfusated through the cannulated intestine segment at flow rate of 0.3 ml/min. Both the mesenteric blood and perfusate were collected into the pre-weighted microtubes every 5 min and lasted for 40 min. The blood samples were centrifugation at 16,000×*g* for 3 min, and the plasma were transferred to another tube. All the perfusate and plasma samples were kept at −80°C until analysis.

In Vitro Intestinal Enzymatic Kinetic Study

The glucuronidation reaction followed our previously described procedure (27). Briefly, a series of concentration of W or OA (0.35–35 μM) were pre-incubated with different subcellular fractions or UGT isozymes in 50 mM Tris–HCl buffer (pH 7.4) containing 8 mM of $MgCl_2$ and 25 μg/ml of alamethicin for 5 min at 37°C. The reaction was initiated by the addition of 2 mM UDPGA. The protein concentrations were 0.2 mg/ml for UGT1A8, UGT1A10, and 0.8 mg/ml was employed for RIS9. The protein concentration was 0.1 mg/ml for HIM. The incubation lasted 10 min for all the reactions except for the reaction in UGT1A8 (5 min). The protein concentrations and incubation times were optimized to ensure linearity for metabolite formation. All the experiments were performed in triplicate.

Similar to the condition of glucuronidation, different concentrations of W or OA (0.35–35 μM) were pre-incubated with RIS9 at a final protein concentration of 0.8 mg/ml at 37°C min in 50 mM Tris–HCl buffer (pH 7.4) containing 5 mM $MgCl_2$, 8 mM dithiothreitol, and 0.0625% bovine serum albumin. The reaction was initiated by addition of 200 μM of PAPS and lasted for 10 min.

All the enzymatic reactions were terminated by the addition of 40 μl of ice cold acetonitrile/acetic acid (9:1, *v/v*) containing 40 μg/ml internal standard (3, 7-dihydroxyflavone). The mixture was centrifuged at 16,000×*g* for 10 min, and the supernatant was directly injected into HPLC/UV system for analysis.

Analytical Methods

For the quantification of W, OA, WG, and OAG, the samples after transport study in Caco-2 and MDCK cell model, *in vitro* enzymatic kinetic study, as well as the perfusate samples after rat *in situ* single-pass intestinal perfusion study were prepared and determined followed the method published previously (28). The blood samples obtained from rat *in situ* single-pass intestinal perfusion study were treated and analyzed according to previous report (29).

Due to lack of commercial availability of standard sulfate of W and OA (WS and OAS), the concentrations of WS and OAS after the transport study in Caco-2 cell monolayer model were quantified indirectly assuming that WS/OAS has the same UV absorbance group as W/OA and one molar of W/OA produce one molar of WS/OAS. As a result, the calibration curve was firstly plotted with the molar concentrations of W/OA *versus* the peak area ratios of W/OA to IS. The molar concentration of WS/OAS was calculated based on their observed peak area ratios from the calibration curve of W/OA.

Data Analysis

The permeability coefficients (P_{app}) of W, OA, WG, and OAG in Caco-2 and MDCK cell monolayer models were calculated as described previously using the following equations (30):

$$P_{app} = [(dC/dt \times V)]/(A \times C)$$

dC/dt change of the drug concentration in the receiver chambers over time
V volume of the solution in the receiver chambers
A membrane surface area
C loading concentration in the donor chambers

Besides, the percentage of metabolism of W and OA during their intestinal absorption in Caco-2 cell monolayer model was calculated according to the following equation, in which "AP" represented cumulative amount in apical side, "BL" represented cumulative amount in basolateral side, and "uptake" represented cell uptake.

$$\%\ \text{of metabolism} = \frac{\Sigma\ \text{metabolite}_{(AP+BL+uptake)}}{\Sigma\ \text{parent drug}_{(AP+BL+uptake)} + \Sigma\ \text{metabolites}_{(AP+BL+uptake)}}$$

For rat *in situ* single-pass intestinal perfusion model, permeability coefficients of parent drugs were calculated based on the appearance and disappearance of compounds in the mesenteric blood (P_{blood}) and the perfusate (P_{lumen}), respectively, according to the following equations:

$$P_{blood} = \frac{dX/dt}{AC_0}$$

(31,32) where dX/dt is the rate of drug appearance in mesenteric blood, A is the area of the perfusated intestine

Table I. Bidirectional Transport Permeability and Metabolism of B/W/OA in Caco-2 Cell Monolayer Model (n=3)

	A to B		B to A	
Loading concentration (μM)	P_{app} (×10^{-6} cm/s)	% of metabolism	P_{app} (×10^{-6} cm/s)	% of metabolism
3.55 (B) (26)	N.D.	N.A.	N.D.	N.A.
7.98 (B) (26)	N.D.	76.9	N.D.	45.3
23.7 (B) (26)	3.80±0.48	51.8	4.03±0.15	26.3
3.79 (W)	N.D.	95.9±2.16	N.D.	53.0±0.34
7.58 (W)	10.5±2.91	53.1±5.13	7.29±1.25	43.8±1.31
18.9 (W)	12.6±0.55	32.1±0.98	8.96±1.36	28.5±1.35
3.47 (OA)	N.D.	99.8±0.02	N.D.	79.0±1.09
6.94 (OA)	2.91±0.44	90.3±0.20	4.43±0.90	67.7±1.14
17.4 (OA)	5.73±0.19	55.6±1.91	5.62±0.55	36.8±1.55

segment, and C_0 is the initial drug concentration in the perfusate buffer.

$$P_{\text{lumen}} = -\frac{Q}{A}\ln\frac{C_{\text{out}}}{C_{\text{in}}}$$

(33) where A is the area of the perfused intestine segment, Q is the perfusion flow rate, C_{in} is the drug concentration in the inlet of the perfusate entering the intestinal segment, and C_{out} is the drug concentration in the exiting perfusate at the steady state.

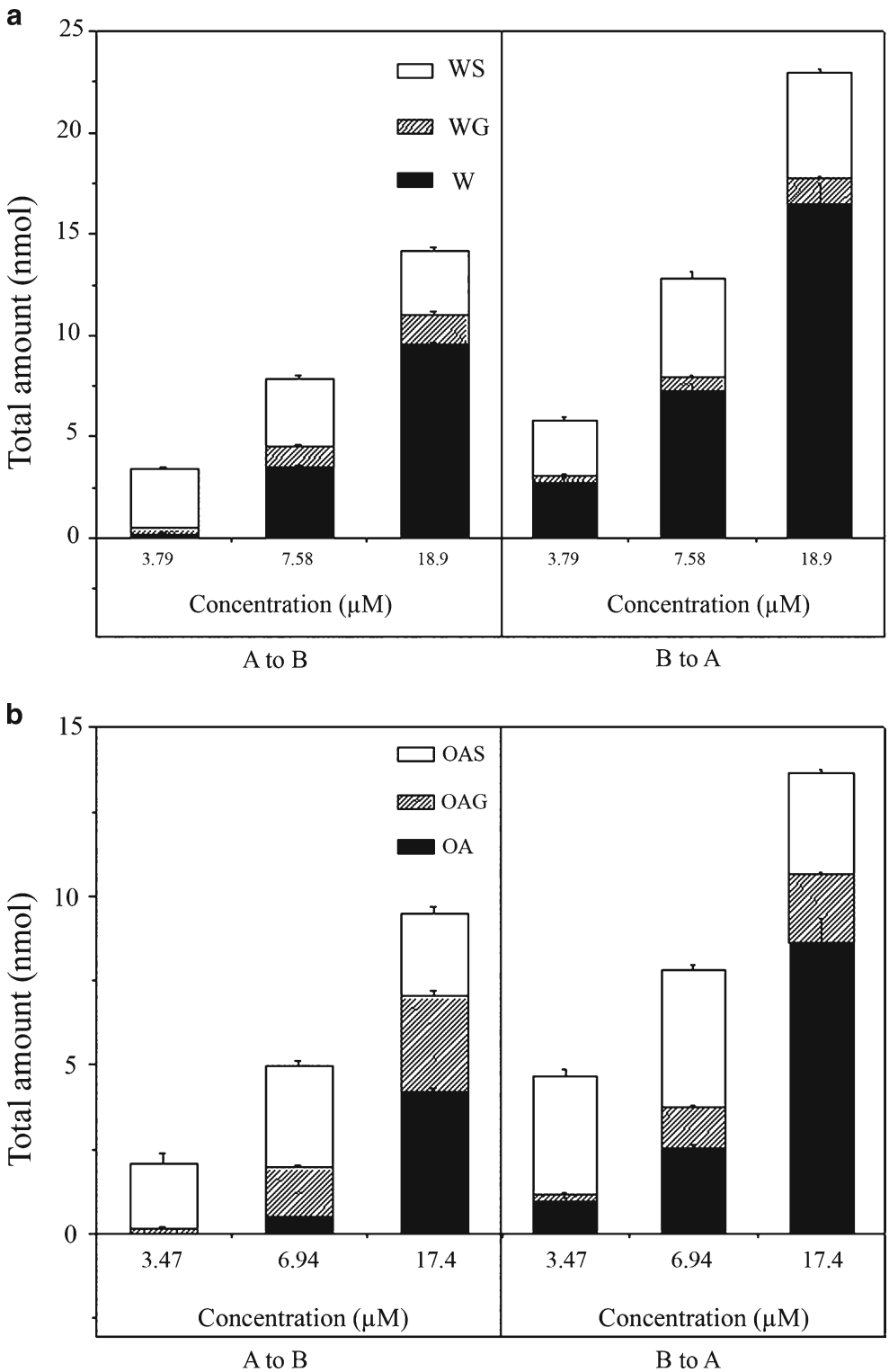

Fig. 2. **a** Total amount of W and its metabolites formed during A to B transport (*left*) and B to A transport of W (*right*) on Caco-2 cell monolayer model. **b** Total amount of OA and its metabolites formed during A to B transport (*left*) and B to A transport of OA (*right*) on Caco-2 cell monolayer model

Cummins's extraction ratio (ER) was employed to evaluate the extent of intestinal metabolism of W and OA (33). Cummins's ER was the ratio of the total amount of metabolites found during the perfusion process divided by a sum of the total amount of metabolites formed and the parent compound present in the mesenteric blood.

$$\mathrm{ER} = \frac{\Sigma\,\mathrm{metabolite}_{(\mathrm{perfusate+blood})}}{\Sigma\,\mathrm{parent\,drug}_{(\mathrm{blood})} + \Sigma\,\mathrm{metabolites}_{(\mathrm{perfusate+blood})}}$$

Reaction rate of glucuronidation in intestinal microsomal fractions and UGT isozymes was expressed as the amount of metabolites formed (nanomoles) per minute per milligram

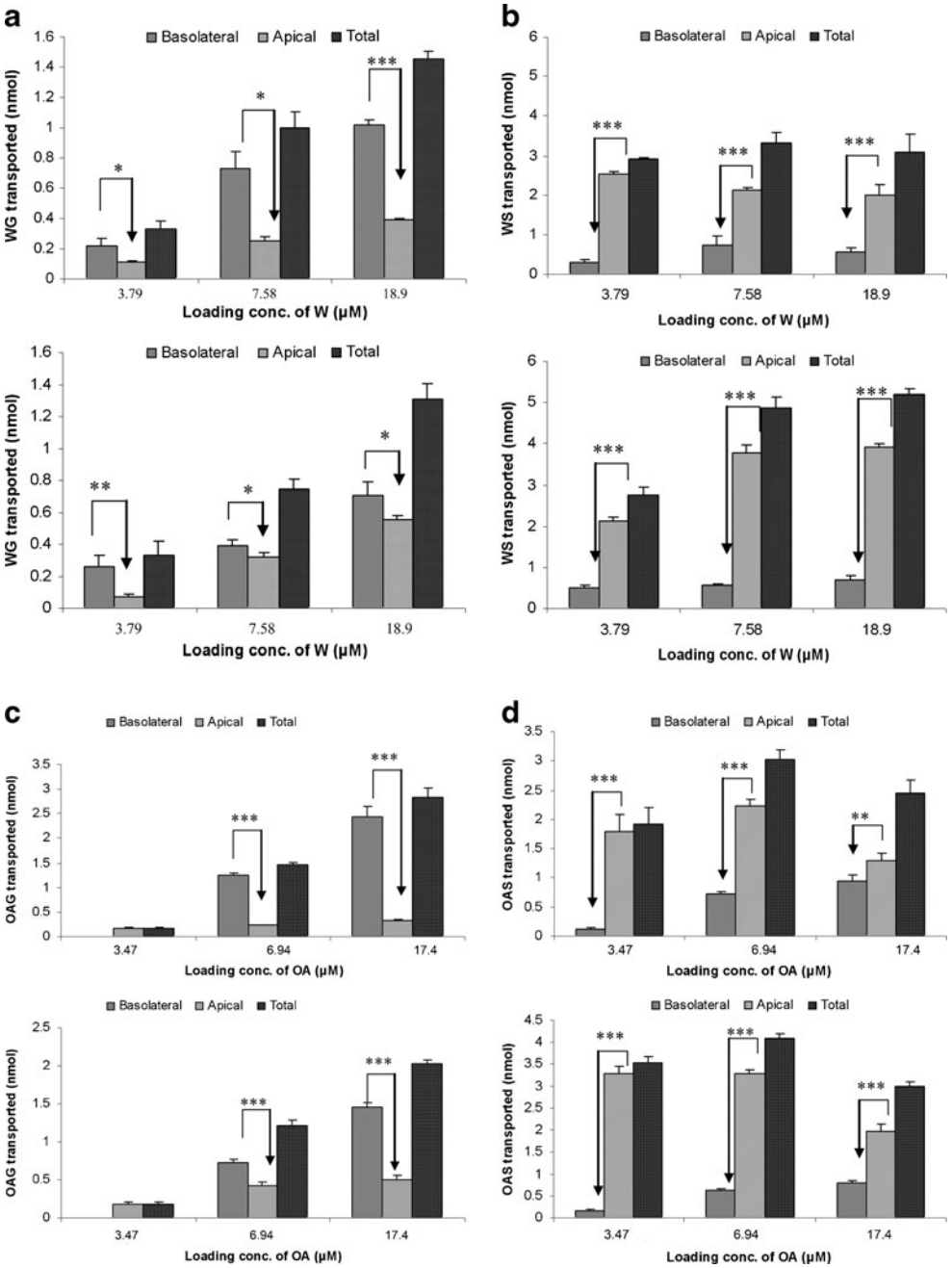

Fig. 3. **a** Efflux transport of WG during bidirectional transport of W at various concentrations: A to B transport (*upper*) and B to A transport (*lower*) in Caco-2 cell monolayer model. **b** Efflux transport of WS during bidirectional transport of W at various concentrations: A to B transport (*upper*) and B to A transport (*lower*) in Caco-2 cell monolayer model. **c** Efflux transport of OAG during bidirectional transport of OA at various concentrations: A to B transport (*upper*) and B to A transport (*lower*) in Caco-2 cell monolayer model. **d** Efflux transport of OAS during bidirectional transport of OA at various concentrations: A to B transport (*upper*) and B to A transport (*lower*) in Caco-2 cell monolayer model. *p <0.05; **p<0.01; ***p<0.001

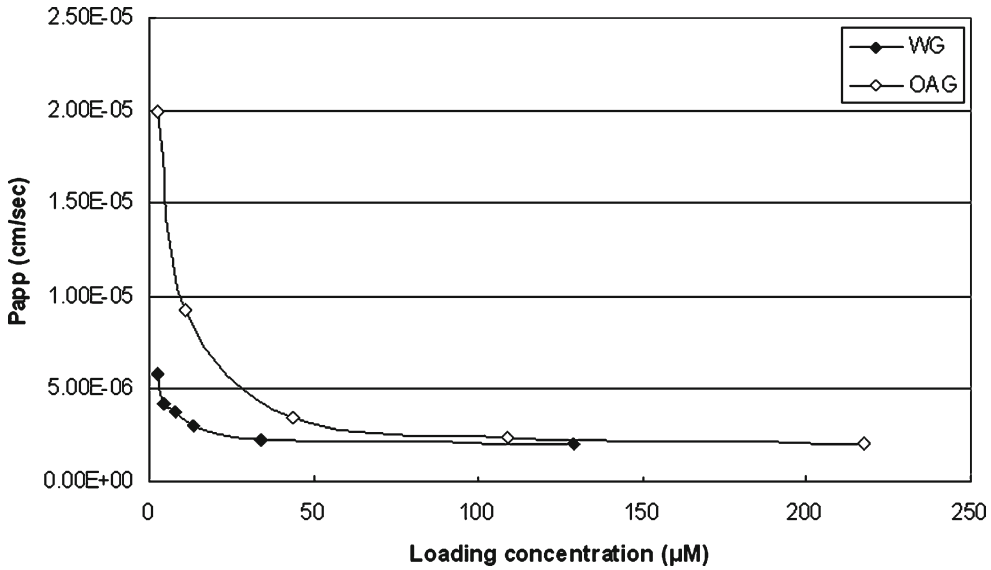

Fig. 4. P_{app} values of WG and OAG in B to A transport at various loading concentrations in Caco-2 cell monolayer model

protein. All the reported values were presented as mean±SE. The enzyme kinetic parameters were obtained by fitting data into the Michaelis–Menten equation using the software of Prism (GraphPad Software, Inc.).

$$\text{Michaelis} - \text{Menten equation}: V = V_{max} \times C/(K_m + C);$$

where V_{max} is the maximal velocity, K_m is the substrate concentration at half maximal velocity, V is the metabolic formation rate, and C is the substrate concentration.

RESULTS

Intestinal Absorption and Disposition of the Three Flavones in Caco-2 Cell Model

The transport and metabolism of W/OA resembled that of B in Caco-2 cell monolayer model (26). All three flavones demonstrated efficient apical to basolateral permeabilities, which are comparable to that of the transcellular marker compounds (30,34) (Table I). At similar loading concentration, *W* demonstrated the highest P_{app} value followed by OA and B.

Similar to what has been observed for B (26), during the bidirectional transport, extensive phase II metabolism has been observed for W/OA in the forms of glucuronidation and sulfation. The glucuronic acid conjugates of W/OA at 7-OH were identified by comparing their HPLC/UV and liquid chromatography with tandem mass spectrometry detection (LC/MS/MS) chromatograms with those of the corresponding authentic standards. The sulfate conjugates of W/OA with molecular ion and major fragment ion appeared at *m/z* 363 and *m/z* 283 (after loss of a sulfate group from its molecular ion), respectively, were identified by LC/MS/MS at negative mode. The amount of the conjugated metabolites increased linearly with time. The percentage of metabolism showed a saturation profile of metabolism for three flavones, which was shown in Table I. At similar loading concentration, OA demonstrated the highest percentage of metabolism among three flavones. By comparing the total amount of conjugated metabolites, it was found that sulfation complied with a saturation profile (Fig. 2a, b). The intracellularly formed glucuronides were preferentially extruded to the basolateral side whereas the formed sulfates were easier to reach the apical side regardless of the side of loading (Fig. 3a–d) (29).

Transport of Glucuronides of Three Flavones in Caco-2 Cell Model and MDCK Cell Model

Comparison of the absorptive transport of the glucuronides of the three flavones found that their apical to basolateral permeabilities were all limited, whereas their

Table II. P_{app} Values During Excretive Transport of WG and OAG at 2.17 μM in Presence and Absence of Various Membrane Transporter Inhibitor/Substrate in Caco-2 Cell Monolayer Model (n=3)

		Verapamil	ES	EG	MTX	MK571
Flavones	Control	P-gp inhibitor	Substrate of MRPs		Substrate of BCRP	Inhibitor of MRPs
BG (26) ($\times 10^{-6}$ cm/s)	5.70±0.34	N.A.	N.A.	3.55±0.16***	N.A.	N.D.***
WG ($\times 10^{-6}$ cm/s)	5.78±0.15	5.76±0.64	N.D.***	4.65±0.34*	5.61±0.16	N.D.***
OAG ($\times 10^{-5}$ cm/s)	1.99±0.18	2.00±0.08	0.66±0.01***	N.A.	2.38±0.09**	N.D.***

N.A. the experiment was not conducted, *N.D.* compound was not detectable at apical side
*$p<0.05$; **$p<0.01$; ***$p<0.001$ compared with control

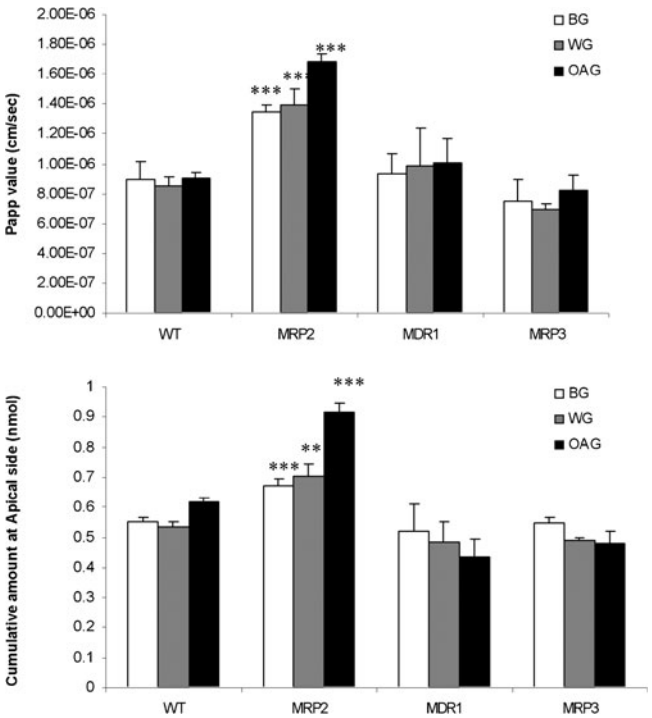

Fig. 5. Cumulative amount at apical side (*upper*) and apparent permeability coefficient (*lower*) of BG/WG/OAG after their basolateral to apical transports in MDCK cell model. ***$p<0.001$

basolateral to apical transport were extensive with saturation reached at concentrations of 50 μM for BG (26), 34.0 μM for WG, and 43.5 μM for OAG (Fig. 4).

Further inhibition on the three corresponding glucuronides in Caco-2 cell model demonstrated that the extent of inhibition varied with different inhibitors. Among the tested inhibitors, MK571 (25 μM) could significantly inhibit the basolateral to apical transport of BG/WG/OAG (Table II) (26), indicating the involvement of MRPs. Furthermore, ES and EG (50 μM) could also reduce the secretive transport of BG/WG/OAG. Nevertheless, the P-gp inhibitors could not significantly affect the basolateral to apical transport of BG/WG/OAG, indicating possibly no involvement of P-gp.

Results of BG/WG/OAG transport study in MDCK cell model were shown in Fig. 5. Comparing with the corresponding results in MDCK/WT, the cumulative amount at apical side of BG/WG/OAG and their P_{app} values were significantly increased only in MDCK/MRP2 cell model (not MDCK/MDR1 and MDCK/MRP3 cell models), indicating significant involvement of MRP2 rather than MDR1 and MRP3 in the efflux transport of BG/WG/OAG.

Intestinal Absorption and Metabolism in Rat *In Situ* Single-Pass Intestinal Perfusion Model

Similar to B (25), W/OA showed favorable permeability across the epithelium of small intestine at 50 μM. The permeability coefficient (P_{lumen}) of B/W/OA determined based on the disappearance of parent drug in the intestinal lumen was calculated to be $1.81\pm0.52\times10^{-4}$ (25), $2.27\pm1.26\times10^{-4}$, and $3.50\pm1.46\times10^{-4}$ cm/s, respectively. In the mesenteric blood samples, the amount of glucuronides of W and OA (WG and OAG) were much higher than their corresponding parent drugs. The permeability coefficient (P_{blood}) of B/W/OA based on the appearance of parent drug in mesenteric blood was calculated to be $3.50\pm2.30\times10^{-6}$ (25), $4.48\pm1.86\times10^{-6}$, and $3.00\pm1.51\times10^{-6}$ cm/s for B, W, and OA, respectively.

Unlike the observation in Caco-2 model, only glucuronides of B/W/OA were detected in both perfusate and mesenteric blood in their rat single-pass intestinal perfusion model studies. The cumulative amount of parent drug and formed glucuronides in mesenteric blood as well as the metabolites in perfusate of the three flavones were summarized in Table III. It was noticed that the amount of formed glucuronides was much higher than that of parent drugs in mesenteric blood. Cummins's extraction ratios of W (0.91±0.03), OA (0.95±0.02), and B (0.96±0.02) (25) indicated similar extensive first-pass glucuronidation in intestine.

Enzymatic Kinetic Profiles of Glucuronidation of B/W/OA in Various Sub-cellular Fractions

The enzymatic kinetic profiles of intestinal glucuronidation of W/OA in HIM, RIS9, UGT1A8, and UGT1A10 were obtained and compared with previous published data on B (27). The formation of BG/WG/OAG at various concentrations followed the Michaelis–Menten equation with favorable goodness of fit ($R^2>0.9$), and the enzymatic kinetic parameters including K_m, V_{max}, and Cl_{int} (V_{max}/K_m) were listed in Table IV. Nevertheless, there was no sulfation observed in RIS9 fraction. Comparing the kinetic parameters among B, W, and OA in HIM and UGT 1A8, it was found that OA showed the highest intrinsic clearance which was almost 10-fold higher than that of B. The results indicated that the formation of glucuronides was the fastest in OA.

DISCUSSION

The current study focused on the comparison of intestinal absorption and metabolism among three major flavones in *Radix Scutellariae* to explore the structure–

Table III. Metabolism of W and OA During Their *In Situ* Single-Pass Intestinal Perfusion in Rat ($n=6$)

	Cumulative amount ($\times10^3$ pmol/com)			
Flavones	Glucuronide in blood	Glucuronide in perfusate	Parent flavone in blood	ER
B (25)	7.24±1.74	8.80±1.58	0.682±0.364	0.96±0.02
W	5.86±1.91	3.20±1.77	0.861±0.408	0.91±0.03
OA	5.26±1.06	5.22±1.19	0.558±0.285	0.95±0.02

activity relationships between their chemical structures and pharmacokinetic profiles. The components of herbal medicines are usually complex, and herbal medicines are usually consumed in herbal mixtures during their clinical applications. Flavonoids are ubiquitous in plants, even in our daily diets (35). Therefore, the chance that these components with similar structures were administrated together is relatively high. Based on our findings on the relationships between the flavonoid structures and their pharmacokinetic behaviors, we indicate the feasibility to predict the *in vivo* fate of those components with similar structures but unknown pharmacokinetics.

The proposed mechanism of intestinal disposition of B/W/OA was demonstrated in Fig. 6. In both *in vitro* and *in situ* absorption models, B/W/OA demonstrated effective permeabilities. The permeabilities of B/W/OA in Caco-2 cell monolayer model were within the range of P_{app} values of drugs with high permeabilities (30). The P_{lumen} of B/W/OA obtained from the *in situ* intestinal perfusion model was comparable to that of the well-absorbed marker, antipyrine (36). At similar loading concentration, W showed the highest P_{app} value followed by OA and then B in Caco-2 cell model. Although such trend was less significant in rat intestinal perfusion model, W also demonstrated higher P_{blood} value than that of B and OA. Based on the software of ALOGPS (version 2.1), the log*P* values of B, W, and OA were calculated to be 2.59, 2.84, and 2.73, while their solubilities in water were 150, 65.3, and 66.6 mg/l, respectively. The log*P* values of the three flavones were in the order of W>OA>B, which is consistent with the rank of their P_{app} values obtained in Caco-2 cell model and rat intestinal perfusion model. Dai *et al*. investigated the intestinal permeabilities of flavonoids including B, W, and OA from Chinese herbal remedy Xiaochaihu-tang across Caco-2 cell monolayers (37), in which two metabolic pathways were also observed for all studied flavone. Their calculated P_{app} values of B and OA at similar loading concentrations were comparable to ours. With regard to W, the calculated P_{app} value by Dai *et al.* was greater than ours. Such discrepancy may probably be due to the saturation of metabolism at a much higher loading concentration (20 μg/ml) in their study, which may lead to more W permeation via passive diffusion.

Extensive metabolisms of three flavones were observed in both models with percentage of metabolism even higher than 90%. In Caco-2 cell model, OA showed the greatest percentage of metabolism, whereas such trend was not significant in the rat intestinal perfusion model. However, the Cummin's extraction ratios for the three flavones were quite similar. Such discrepancy in the observations between the two absorption model could be due to the higher exposure of drugs toward intestinal enzymes in rat *in situ* intestinal perfusion model (38).

As for the pathways of metabolism, B, W, and OA behaved differently in different models. In Caco-2 cell monolayer model, W and OA underwent glucuronidation and sulfation. Nevertheless, more types of metabolites were observed for B, indicating that B is more vulnerable to be metabolized than the other two flavones. In addition to BG and BS, there were OAG, OAS, and even OA observed in the bidirectional transport samples after high concentration of B (50 μM) was loaded (data not shown here). It was proposed

Table IV. Enzyme Kinetic Parameters of the Glucuronidation for B/W/OA in Various Intestinal Fractions and UGTs ($n=3$)

Fraction/ UGT	B			W			OA		
	V_{max} (nmol/min/mg)	K_m (μM)	Cl_{int} ($\times 10^3$ μl/min/mg)	V_{max} (nmol/min/mg)	K_m (μM)	Cl_{int} ($\times 10^3$ μl/min/mg)	V_{max} (nmol/min/mg)	K_m (μM)	Cl_{int} ($\times 10^3$ μl/min/mg)
HIM	41.9±1.92 (27)	93.9±7.71 (27)	0.446 (27)	5.13±0.16	1.23±0.17	4.17	5.24±0.24	1.04±0.23	5.04
RIS9	6.15±0.85	46.7±10.2	0.131	8.05±0.56	44.0±4.85	0.182	3.87±0.14	9.95±0.96	0.388
1A8	3.17±0.27 (27)	19.5±4.80 (27)	0.163 (27)	8.86±0.54	9.37±1.54	0.945	7.65±0.75	6.96±1.99	1.10
1A10	0.38±0.03	5.40±1.49	0.710	5.21 ±0.29	12.1±1.61	0.431	7.29±0.33	4.81±0.68	1.52

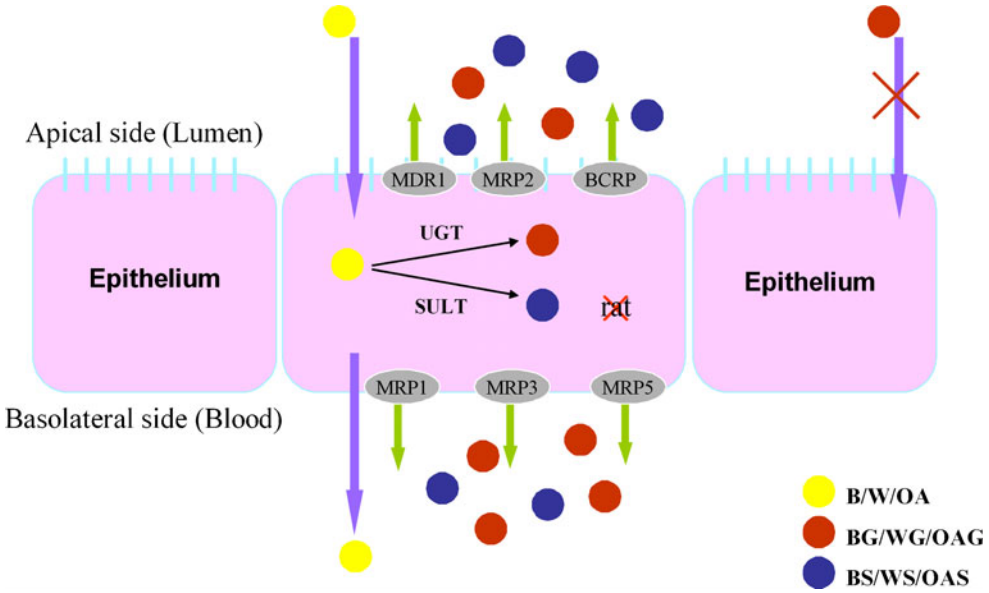

Fig. 6. Proposed mechanisms for the intestinal absorptions and dispositions of B/W/OA

that B was firstly metabolized into OA by methylation (39), and then the formed OA was further glucuronidated and sulfated into OAG and OAS. In rat intestinal perfusion model, only glucuronidation was observed for the three flavones, indicating that species difference occurred with regard to the intestinal metabolism of B/W/OA. In order to further confirm the species difference in sulfation of B/W/OA between animal models and human, experiments involving both human intestinal fractions and mice intestinal perfusion model are needed (40). Again, the differences in the chemical structures of the three flavones, especially the number and position of hydroxyl and methoxy groups might contribute to the differences in the pathways and extent of metabolism among B, W, and OA. For B, there are two hydroxyl groups at A-ring. Considering what have been observed in Caco-2 cell model, it could be suggested that 7-OH and 6-OH are more readily to be glucuronidated and methylated, respectively. The arrangement of hydroxyl and methoxy groups at A-ring produces lower stereospecific blockade in OA than W, which might contribute to the higher extent of glucuronidation of OA.

In vitro enzymatic kinetics study was further employed to investigate the intestinal metabolism of B/W/OA. In the extrahepatic organs, UGT 1A8 and UGT 1A10 are expressed in the gastrointestinal tract (41,42). Based on previous investigations on B from us and others (27,43), UGT 1A8 and UGT 1A10 as well as HIM and RIS9 were chosen as subcellular fractions to investigate the intestinal glucuronidation of W and OA and compared with that of B. Zhou *et al.* demonstrated that UGT1A8 and UGT1A10 contributed to the intestinal glucuronidation of W and OA (43). However, different kinetic profiles were observed in their study. The kinetic profile of UGT1A8 and UGT1A10 mediated glucuronidation complied with auto-activation kinetics for W. Glucuronidation of OA followed classic Michaelis–Menten profile in UGT1A10, whereas it followed auto-activation kinetics in UGT1A8. Such different enzyme kinetic profiles from ours might be due to different incubation time employed in the studies. In our study, an optimized incubation time of 10 min was used, whereas 1-h incubation was adopted in their study. Since UGT is a superfamily of microsomal enzymes and involved in the detoxification of xenobiotics, its polymorphism would have the toxicological or pharmacological consequences. For UGT1A subfamily, it comprises 12 promoters and first exons and encodes nine enzymes including UGTs 1A1, 1A3, 1A4, 1A5, 1A6, 1A7, 1A8, 1A9, and 1A10 (44). Recently, there have been a number of studies reporting the polymorphism of UGT1A subfamily that could result in their activities of glucuronidation and related pharmacodynamic effects. For example, higher V_{max}, K_m, and intrinsic clearance were observed for the single nucleotide polymorphisms of UGT1A9 (C3Y, 8G>A) (45). Polymorphism of UGT1A7 was associated with lung cancer and liver cirrhosis (46,47). Nevertheless, the study about the polymorphism of UGT1A8 and UGT1A10 is limited. Based on previous studies of other UGTs, the polymorphism of UGT1A8 and UGT1A10 could not be excluded at the current stage.

For the study of intestinal sulfation, due to the unavailability of intestinal human cub-cellular fractions, it was only carried out in RIS9 at this stage. Again, there was no reaction of three flavones, which was consistent to the result in rat intestinal perfusion model. Interestingly, differences were also observed among B, W, and OA with respect to liver glucuronidation. After oral administration of pure W and proprietary traditional Chinese formulation containing W, there was an additional glucuronide of W detected in addition to WG (29). Besides, we found that B, W, and OA exhibited different enzymatic kinetic profiles in UGT 1A3 (Fig. 7). The profile of B could be fitted by typical Michaelis–Menten equation, whereas the profiles of W and OA complied with a substrate inhibition profile. It was reported that the number of hydroxyl and methoxy group could significantly contribute to the affinity of flavonoids toward UGT 1A3 (48,49). As a result, the existence of methoxy group and the difference in chemical structures might contribute to the different kinetic profiles of B, W, and OA.

Intracellularly formed phase II metabolites were generally effluxed out of the cells by membrane transporters. Based on the results from transport study of B/W/OA, it was

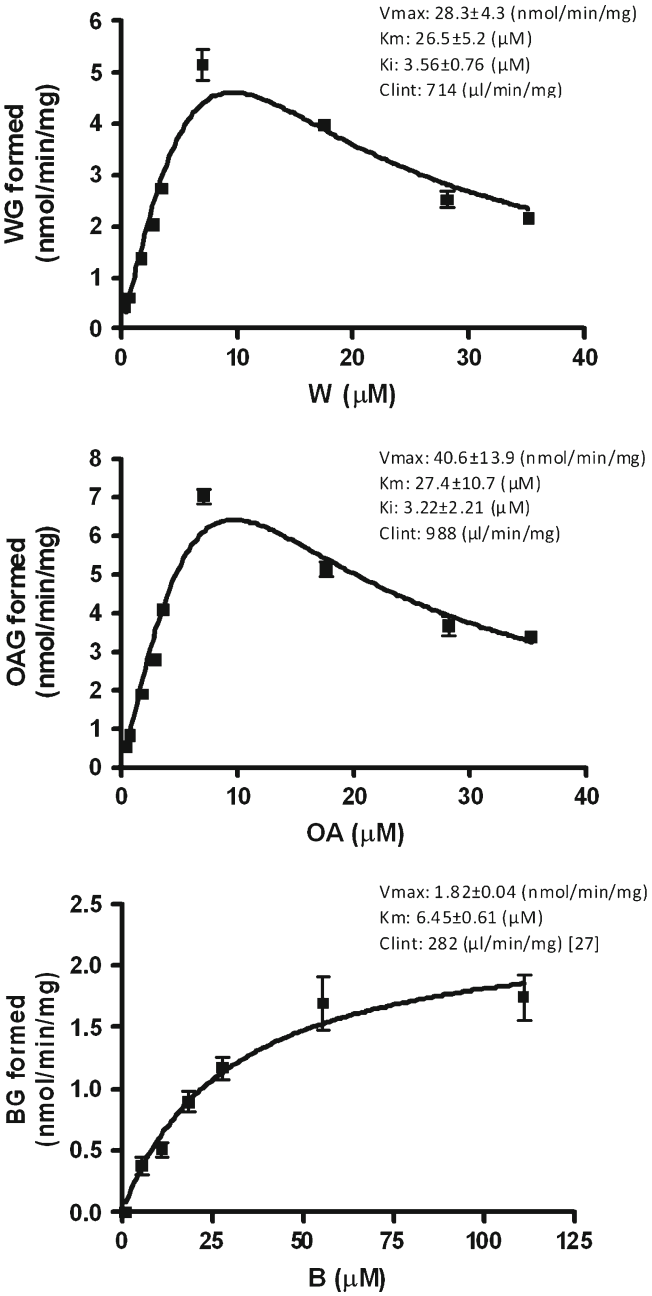

Fig. 7. Formation rate of WG (*upper*), OAG (*middle*), and BG (*lower*) *versus* substrate concentration plots for UGT1A3

proposed that glucuronides have higher affinity to the basolateral transporters such as MRP1, MRP3, and MRP5, and the efflux of sulfates was mediated by apical transporters such as P-gp, MRP2, and BCRP (50,51). Furthermore, the basolateral to apical transport studies of BG/WG/OAG were conducted in the presence of transporter inhibitors or substrates including verapamil (52,53), MK571 (54,55), EG and ES (56–59), and MTX (60,61). The results strongly suggested that MRPs and BCRP might be involved in the efflux of conjugated metabolites of the glucuronides. In addition, basolateral to apical transport study of BG/WG/OAG was conducted in the transfected MDCK cell lines with human transporter genes. It was found that the permeabilities of BG/OAG/WG were all significantly increased in MDCK/MRP2 cell model rather than MDCK/MDR1 and MDCK/MRP3 cell models, indicating the important role of MRP2. Nevertheless, our bidirectional transport studies of B/W/OA in Caco-2 cells found that the intracellularly formed glucuronides showed preference to the basolateral transporters, which was contradictory with the results from the MDCK cell models. Competition in binding to the apical transporters such as MRP2 and BCRP *versus* basolateral transporters such as MRP1 and MRP5 in the two absorption models should be further investigated in order to explain such discrepancy in the preference of allocations of the three formed glucuronides from two cell models.

CONCLUSIONS

Three studied flavones from RS were readily absorbed with similar intestinal permeabilities. However, the extent of the intestinal glucuronidation and dispositions during their intestinal absorption varied. OA exhibited the highest intrinsic clearance among three flavones. The number and position of hydroxyl as well as methoxy group might account for the different intestinal absorption and disposition metabolism among B, W, and OA.

ACKNOWLEDGMENTS

The authors are grateful for CUHK478607 and CUHK480010 from the Research Grants Council of the Hong Kong SAR, China.

REFERENCES

1. Shang X, He X, He X, Li M, Zhang R, Fan P, *et al*. The genus *Scutellaria* an ethnopharmacological and phytochemical review. J Ethnopharmacol. 2010;128:279–313.
2. Chen Y, Yang L, Lee TJ. Oroxylin A inhibition of lipopolysaccharide-induced iNOS and COX-2 gene expression via suppression of nuclear factor-kappaB activation. Biochem Pharmacol. 2000;59:1445–57.
3. Chi YS, Lim H, Park H, Kim HP. Effects of wogonin, a plant flavone from Scutellaria radix, on skin inflammation: *in vivo* regulation of inflammation-associated gene expression. Biochem Pharmacol. 2003;66:1271–8.
4. Woo KJ, Lim JH, Suh SI, Kwon YK, Shin SW, Kim SC, *et al.* Differential inhibitory effects of baicalein and baicalin on LPS-induced cyclooxygenase-2 expression through inhibition of C/EBPbeta DNA-binding activity. Immunobiology. 2006;211:359–68.
5. Lee WR, Shen SC, Lin HY, Hou WC, Yang LL, Chen YC. Wogonin and fisetin induce apoptosis in human promyeloleukemic cells, accompanied by a decrease of reactive oxygen species, and activation of caspase 3 and Ca(2+)-dependent endonuclease. Biochem Pharmacol. 2002;63:225–36.
6. Sun Y, Lu N, Ling Y, Gao Y, Chen Y, Wang L, *et al.* Oroxylin A suppresses invasion through down-regulating the expression of matrix metalloproteinase-2/9 in MDA-MB-435 human breast cancer cells. Eur J Pharmacol. 2009;603:22–8.
7. Ahn HC, Lee SY, Kim JW, Son WS, Shin CG, Lee BJ. Binding aspects of baicalein to HIV-1 integrase. Mol Cells. 2001;12:127–30.
8. Guo Q, Zhao L, You Q, Yang Y, Gu H, Song G, *et al.* Anti-hepatitis B virus activity of wogonin *in vitro* and *in vivo*. Antiviral Res. 2007;74:16–24.
9. Wohlfarth C, Efferth T. Natural products as promising drug candidates for the treatment of hepatitis B and C. Acta Pharmacol Sin. 2009;30:25–30.
10. Huen MS, Leung JW, Ng W, Lui WS, Chan MN, Wong JT, *et al.* 5,7-Dihydroxy-6-methoxyflavone, a benzodiazepine site ligand

isolated from *Scutellaria baicalensis* Georgi, with selective antagonistic properties. Biochem Pharmacol. 2003;66:125–32.
11. Hwang YS, Shin CY, Huh Y, Ryu JH. Hwangryun-Hae-Dok-tang (Huanglian-Jie-Du-Tang) extract and its constituents reduce ischemia–reperfusion brain injury and neutrophil infiltration in rats. Life Sci. 2002;71:2105–17.
12. Kim DH, Jeon SJ, Son KH, Jung JW, Lee S, Yoon BH, *et al*. The ameliorating effect of oroxylin A on scopolamine-induced memory impairment in mice. Neurobiol Learn Mem. 2007;87:536–46.
13. Hui KM, Huen MS, Wang HY, Zheng H, Sigel E, Baur R, *et al*. Anxiolytic effect of wogonin, a benzodiazepine receptor ligand isolated from *Scutellaria baicalensis* Georgi. Biochem Pharmacol. 2002;64:1415–24.
14. Liao JF, Hung WY, Chen CF. Anxiolytic-like effects of baicalein and baicalin in the Vogel conflict test in mice. Eur J Pharmacol. 2003;464:141–6.
15. Peterson MD, Mooseker MS. Characterization of the enterocyte-like brush border cytoskeleton of the C2BBe clones of the human intestinal cell line, Caco-2. J Cell Sci. 1992;102(Pt 3):581–600.
16. Darnell M, Karlsson JE, Owen A, Hidalgo IJ, Li J, Zhang W, *et al*. Investigation of the involvement of P-glycoprotein and multidrug resistance-associated protein 2 in the efflux of ximelagatran and its metabolites by using short hairpin RNA knockdown in Caco-2 cells. Drug Metab Dispos. 2010;38:491–7.
17. Hirohashi T, Suzuki H, Chu XY, Tamai I, Tsuji A, Sugiyama Y. Function and expression of multidrug resistance-associated protein family in human colon adenocarcinoma cells (Caco-2). J Pharmacol Exp Ther. 2000;292:265–70.
18. Hunter J, Jepson MA, Tsuruo T, Simmons NL, Hirst BH. Functional expression of P-glycoprotein in apical membranes of human intestinal Caco-2 cells. Kinetics of vinblastine secretion and interaction with modulators. J Biol Chem. 1993;268:14991–7.
19. Kobayashi D, Nozawa T, Imai K, Nezu J, Tsuji A, Tamai I. Involvement of human organic anion transporting polypeptide OATP-B (SLC21A9) in pH-dependent transport across intestinal apical membrane. J Pharmacol Exp Ther. 2003;306:703–8.
20. Paine MF, Fisher MB. Immunochemical identification of UGT isoforms in human small bowel and in Caco-2 cell monolayers. Biochem Biophys Res Commun. 2000;273:1053–7.
21. Siissalo S, Laine L, Tolonen A, Kaukonen AM, Finel M, Hirvonen J. Caco-2 cell monolayers as a tool to study simultaneous phase II metabolism and metabolite efflux of indomethacin, paracetamol and 1-naphthol. Int J Pharm. 2010;383:24–9.
22. Siissalo S, Zhang H, Stilgenbauer E, Kaukonen AM, Hirvonen J, Finel M. The expression of most UDP-glucuronosyltransferases (UGTs) is increased significantly during Caco-2 cell differentiation, whereas UGT1A6 is highly expressed also in undifferentiated cells. Drug Metab Dispos. 2008;36:2331–6.
23. Sun D, Lennernas H, Welage LS, Barnett JL, Landowski CP, Foster D, *et al*. Comparison of human duodenum and Caco-2 gene expression profiles for 12,000 gene sequences tags and correlation with permeability of 26 drugs. Pharm Res. 2002;19:1400–16.
24. Cook TJ, Shenoy SS. Intestinal permeability of chlorpyrifos using the single-pass intestinal perfusion method in the rat. Toxicology. 2003;184:125–33.
25. Zhang L, Lin G, Chang Q, Zuo Z. Role of intestinal first-pass metabolism of baicalein in its absorption process. Pharm Res. 2005;22:1050–8.
26. Zhang L, Lin G, Kovacs B, Jani M, Krajcsi P, Zuo Z. Mechanistic study on the intestinal absorption and disposition of baicalein. Eur J Pharm Sci. 2007;31:221–31.
27. Zhang L, Lin G, Zuo Z. Involvement of UDP-glucuronosyltransferases in the extensive liver and intestinal first-pass metabolism of flavonoid baicalein. Pharm Res. 2007;24:81–9.
28. Li C, Zhou L, Lin G, Zuo Z. Contents of major bioactive flavones in proprietary traditional Chinese medicine products and reference herb of radix Scutellariae. J Pharm Biomed Anal. 2009;50:298–306.
29. Li C, Zhang L, Lin G, Zuo Z. Identification and quantification of baicalein, wogonin, oroxylin A and their major glucuronide conjugated metabolites in rat plasma after oral administration of Radix scutellariae product. J Pharm Biomed Anal. 2010;54:750–8.
30. Artursson P, Karlsson J. Correlation between oral drug absorption in humans and apparent drug permeability coefficients in human intestinal epithelial (Caco-2) cells. Biochem Biophys Res Commun. 1991;175:880–5.
31. Amidon GL, Leesman GD, Elliott RL. Improving intestinal absorption of water-insoluble compounds: a membrane metabolism strategy. J Pharm Sci. 1980;69:1363–8.
32. Johnson BM, Chen W, Borchardt RT, Charman WN, Porter CJ. A kinetic evaluation of the absorption, efflux, and metabolism of verapamil in the autoperfused rat jejunum. J Pharmacol Exp Ther. 2003;305:151–8.
33. Cummins CL, Salphati L, Reid MJ, Benet LZ. *In vivo* modulation of intestinal CYP3A metabolism by P-glycoprotein: studies using the rat single-pass intestinal perfusion model. J Pharmacol Exp Ther. 2003;305:306–14.
34. Yee S. *In vitro* permeability across Caco-2 cells (colonic) can predict *in vivo* (small intestinal) absorption in man—fact or myth. Pharm Res. 1997;14:763–6.
35. Hollman PCH, Katan MB. Absorption, metabolism and health effects of dietary flavonoids in man. Biomed Pharmacother. 1997;51:305–10.
36. Fagerholm U, Johansson M, Lennernas H. Comparison between permeability coefficients in rat and human jejunum. Pharm Res. 1996;13:1336–42.
37. Dai JY, Yang JL, Li C. Transport and metabolism of flavonoids from Chinese herbal remedy Xiaochaihu-tang across human intestinal Caco-2 cell monolayers. Acta Pharmacol Sin. 2008;29:1086–93.
38. Shah P, Jogani V, Bagchi T, Misra A. Role of Caco-2 cell monolayers in prediction of intestinal drug absorption. Biotechnol Prog. 2006;22:186–98.
39. Zhang L, Li CR, Lin G, Krajcsi P, Zuo Z. Hepatic metabolism and disposition of baicalein via the coupling of conjugation enzymes and transporters-*in vitro* and *in vivo* evidences. AAPSJ. 2010. doi:10.1208/s12248-011-9277-6.
40. Zhu W, Xu H, Wang SW, Hu M. Breast cancer resistance protein (BCRP) and sulfotransferases contribute significantly to the disposition of genistein in mouse intestine. AAPSJ. 2010;12:525–36.
41. Cheng Z, Radominska-Pandya A, Tephly TR. Cloning and expression of human UDP-glucuronosyltransferase (UGT) 1A8. Arch Biochem Biophys. 1998;356:301–5.
42. Strassburg CP, Oldhafer K, Manns MP, Tukey RH. Differential expression of the UGT1A locus in human liver, biliary, and gastric tissue: identification of UGT1A7 and UGT1A10 transcripts in extrahepatic tissue. Mol Pharmacol. 1997;52:212–20.
43. Zhou Q, Zheng Z, Xia B, Tang L, Lv C, Liu W, *et al*. Use of isoform-specific UGT metabolism to determine and describe rates and profiles of glucuronidation of wogonin and oroxylin A by human liver and intestinal microsomes. Pharm Res. 2010;27:1568–83.
44. Miners JQ, McKinnon RA, Mackenzie PI. Genetic polymorphisms of UDP-glucuronosyltransferases and their functional significance. Toxicology. 2002;27:453–6.
45. Wang H, Yuan L, Zeng S. Characterizing the effect of UDP-glucuronosyltransferase (UGT) 2B7 and UGT1A9 genetic polymorphisms on enantioselective glucuronidation of flurbiprofen. Biochem Pharmacol. 2011;82:1757–63.
46. Araki J, Kobayashi Y, Iwasa M, Urawa N, Gabazza EC, Taquchi O, Kaito M, Adachi Y. Polymorphism of UDP-glucuronosyltransferase 1A7 gene: a possible new risk factor for lung cancer. Eur J Cancer. 2005;41:2360–5.
47. Tang KS, Lee CM, Teng HC, Huang MJ, Huang CS. UDP-glucuronosyltransferase 1A7 polymorphisms are associated with liver cirrhosis. Biochem Biophys Res Commun. 2008;366:643–8.
48. Chen Y, Xie S, Chen S, Zeng S. Glucuronidation of flavonoids by recombinant UGT1A3 and UGT1A9. Biochem Pharmacol. 2008;76:416–25.
49. Xie SG, Chen YK, Zhang W, Chen S, Zeng S. QSMR studies on glucuronidation of flavonoids catalyzed by human UGT 1A3. Chin Pharm J. 2007;42:1505–8.
50. Brand W, Schutte ME, Williamson G, van Zanden JJ, Cnubben NH, Groten JP, *et al*. Flavonoid-mediated inhibition of intestinal ABC transporters may affect the oral bioavailability of drugs, food-borne toxic compounds and bioactive ingredients. Biomed Pharmacother. 2006;60:508–19.
51. Morris ME, Zhang S. Flavonoid–drug interactions: effects of flavonoids on ABC transporters. Life Sci. 2006;78:2116–30.

52. Bansal T, Mishra G, Jaggi M, Khar RK, Talegaonkar S. Effect of P-glycoprotein inhibitor, verapamil, on oral bioavailability and pharmacokinetics of irinotecan in rats. Eur J Pharm Sci. 2009;36:580–90.
53. Wang JC, Liu XY, Lu WL, Chang A, Zhang Q, Goh BC, *et al*. Pharmacokinetics of intravenously administered stealth liposomal doxorubicin modulated with verapamil in rats. Eur J Pharm Biopharm. 2006;62:44–51.
54. Bousquet L, Pruvost A, Didier N, Farinotti R, Mabondzo A. Emtricitabine: inhibitor and substrate of multidrug resistance associated protein. Eur J Pharm Sci. 2008;35:247–56.
55. Videmann B, Tep J, Cavret S, Lecoeur S. Epithelial transport of deoxynivalenol: involvement of human P-glycoprotein (ABCB1) and multidrug resistance-associated protein 2 (ABCC2). Food Chem Toxicol. 2007;45:1938–47.
56. Campbell SD, de Morais SM, Xu JJ. Inhibition of human organic anion transporting polypeptide OATP 1B1 as a mechanism of drug-induced hyperbilirubinemia. Chem Biol Interact. 2004;150:179–87.
57. Hagenbuch B. Cellular entry of thyroid hormones by organic anion transporting polypeptides. Best Pract Res Clin Endocrinol Metab. 2007;21:209–21.
58. Leslie EM, Deeley RG, Cole SP. Multidrug resistance proteins: role of P-glycoprotein, MRP1, MRP2, and BCRP (ABCG2) in tissue defense. Toxicol Appl Pharmacol. 2005;204:216–37.
59. Tiwari AK, Sodani K, Wang SR, Kuang YH, Ashby Jr CR, Chen X, *et al*. Nilotinib (AMN107, Tasigna) reverses multidrug resistance by inhibiting the activity of the ABCB1/Pgp and ABCG2/BCRP/MXR transporters. Biochem Pharmacol. 2009;78:153–61.
60. Mahringer A, Delzer J, Fricker G. A fluorescence-based *in vitro* assay for drug interactions with breast cancer resistance protein (BCRP, ABCG2). Eur J Pharm Biopharm. 2009;72:605–13.
61. Rosenberg MF, Bikadi Z, Chan J, Liu X, Ni Z, Cai X, *et al*. The human breast cancer resistance protein (BCRP/ABCG2) shows conformational changes with mitoxantrone. Structure. 2010;18:482–93.